Available online at www.sciencedirect.com
ScienceDirect
Trans. Nonferrous Met. Soc. China 33(2023) 1893−1905
Transactions of Nonferrous Metals Society of China
www.tnmsc.cn

Arch model of roof and optimization of roof-contacted filling rate in two-step mining

Ming TAO, Yan ZHAO, Jiang GUO

School of Resources and Safety Engineering, Central South University, Changsha 410083, China

Received 10 February 2022; accepted 11 May 2022

Abstract: To investigate the reasonable roof-contacted filling rate (RCFR) of the backfill in the goaf of a deep mine, the three-hinged arch mechanics model was applied to the two-step mine, and the stress expressions of the goaf roof with different roof-contacted filling rates were derived. Then, the influence of RCFR on the stress state of the roof was analyzed combined with numerical simulation. The results indicated that vertical stress changed the stress state of the roof in the room-stopes and pillar-stopes, while horizontal stress mainly affected the stress state of the roof in the room-stopes. The RCFR in the room-stopes had a greater influence on the formation of the self-stable arch of the roof in pillar-stopes. During the mining process of the Dongguashan Copper Mine, the actual RCFR at the site was about 80%, which achieved a safe and stable uninterrupted recovery of mineral resources.

Key words: arch mechanical model; roof-contacted filling rate; roof stability; numerical simulation; two-step mining

1 Introduction

When the underground mineral resources are recovered, there will be different ranges of goaf. Once the goaf instability occurs, it will destroy the production equipment, seriously affect the production progress and even cause casualties [1−3]. Underground pressure and rock strata control are essential to ensure the stability of the goaf. A large number of studies have developed theories and put forward various hypotheses to describe the form of rock strata movement through the conclusion of field projects and laboratory tests [4,5], such as the cantilever beam hypothesis [6], pressure arch hypothesis [7], articulated rock hypothesis [8], voussoir beam theory [9,10], and key layer hypothesis [11,12]. These theories provide theoretical guidance for stope layout, mining sequence, and pillar retention in the mining area [13,14]. Especially, in the mining of shallow mineral resources, retaining ore pillars can effectively control rock strata movement and manage underground pressure [15,16]. However, with the increase in mining depth, the instability risk of pillars under the action of high in-situ stress increases sharply, which is challenging to ensure the stability of goaf [17,18]. As increasing the width of the pillar, the recovery efficiency of mineral resources and the economic benefits of the mine will be reduced. Therefore, it is vital to fill the mine, control the rock strata movement through the backfill, maximize the recovery of mining resources and eliminate the geological disasters caused by the goaf [19]. At the same time, filling the tailings into the underground can also save the tailings storage place, minimize the pollution of tailings to the surrounding environment and facilitate ecologically sustainable development [20−23].

With the wide application of filling mining technology, a large number of studies have been carried out to explore the backfill effect on retaining the stability of goaf in terms of different perspectives. It was reported that backfill improved

Corresponding author: Jiang GUO, Tel: +86-13548599180, E-mail: guojiang@csu.edu.cn
DOI: 10.1016/S1003-6326(23)66230-2

the mechanical properties of the pillar [24,25], owing to its restriction of lateral deformation of the pillar [26], enhancement of the peak strength, and the bearing capacity of the pillar [27]. The results indicated that the backfill not only enhanced the bearing capacity of the pillar, but also supported the roof and effectively controlled the movement of the rock strata [28]. ZHU et al [29] studied the influence of filling material porosity on the filling effect and concluded that putting the filling material under initial compaction before backfilling was the key to controlling rock strata movement by reducing the filling material porosity. FENG et al [30] analyzed the influence of backfill strength on the roof movement, stress distribution, and elastic strain energy evolution law at the mining face, and considered that improving the filling material strength could effectively control the roof subsidence of the mining face and minimize the risk of rock bursts. In addition, the supporting effect of the filling material on the roof is also related to the contact area between them. However, the studies in this regard are still based on similar simulation experiments [31], and the relevant mechanical quantitative studies are still limited. JIANG et al [32] established a three-hinged arch roof model of a single goaf and studied the effect of roof-contacted filling rate (RCFR) on roof stability. However, mining is a continuous process, and the mining and filling of the previous stope will have an impact on the subsequent stope.

Therefore, in this study, the three-hinged arch model was applied to two-step mining to explore the control effect of RCFR on roof rock strata movement during continuous mining and filling. Taking the Dongguashan Copper Mine as an example, the theoretical findings were verified by numerical simulation and field practice. The results of the study will assist in determining a reasonable value of RCFR during continuous mining and provide theoretical guidance for the control of goaf.

2 Project overview

The Dongguashan Copper Deposit is located at 7.5 km east of Tongling City, Anhui Province, China. It is a typical deep deposit, and most of the ore bodies are below −730 m [33]. The ore body is mainly composed of ores such as copper-bearing serpentinite and copper-bearing pyrite. The lithology of the roof is mainly marble, and the floor is distributed with siltstone and diorite. The ore body and floor joints fissures are not developed and have good stability, while the mechanical properties of the roof are relatively poor due to the presence of partial fissures.

In the mines, the staged open stope and subsequent filling mining method with reserved panel barrier pillars are adopted for mining. A panel is divided every 100 m along with the trend of the ore body, and about 20 m barrier pillars are reserved between the panels to enhance the safety of mining and reduce the interaction between panel mining, as shown in Fig. 1. In the panel, the room-stopes and pillar-stopes are alternately distributed along with the vertical ore body trend. The first step is mining room-stopes and then filling them with cemented full tailings. The second step is to mine the pillar-stopes, which are filled with full tailings after mining. This mining sequence is also called two-step mining.

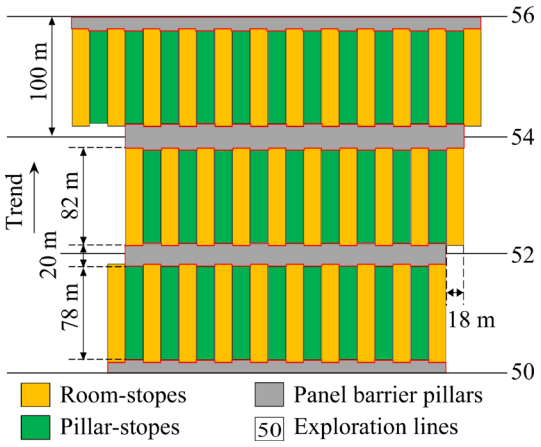

Fig. 1 Layout of some panels and stopes

In the process of mining and filling, the RCFR refers to the ratio of the contact area between the backfill and the roof to the initial unsupported area of the roof. Theoretically, with the improvement in the RCFR, the support capacity of this backfill is enhanced, and the safety of subsequent mining is higher. However, due to the fluidity of filling materials, the increase of the RCFR will inevitably lead to an increase in filling times, an improvement in filling technical difficulty, and a reduction in economic benefits. Therefore, having an economic and reasonable RCFR value on the premise of ensuring mining safety is an urgent problem to be solved in filling mining.

3 Mechanical model of roof in two-step mining and optimization of roof-contacted filling rate

3.1 Self-stable arch model of roof in one-step mining

During one-step mining, goaf will be formed within a certain range. Under the condition of no support, the roof strata in goaf will become suspended. Under the action of self-weight stress in the vertical direction and tectonic stress in the horizontal direction, the roof strata change from compression state to tension state. It is known that the tensile strength of rock mass is far less than the compressive strength, and the roof rock mass will be damaged under the tensile stress, resulting in partial rock mass collapse, and then the roof stress state will be redistributed [34,35]. The engineering practice results show that with the aggravation of the caving phenomenon, the roof surrounding rock will form a caving area within the arch range. Then, a rock arch with pressure bearing structure will be formed at the upper part of the caving area, also known as natural arch, as shown in Fig. 2(a).

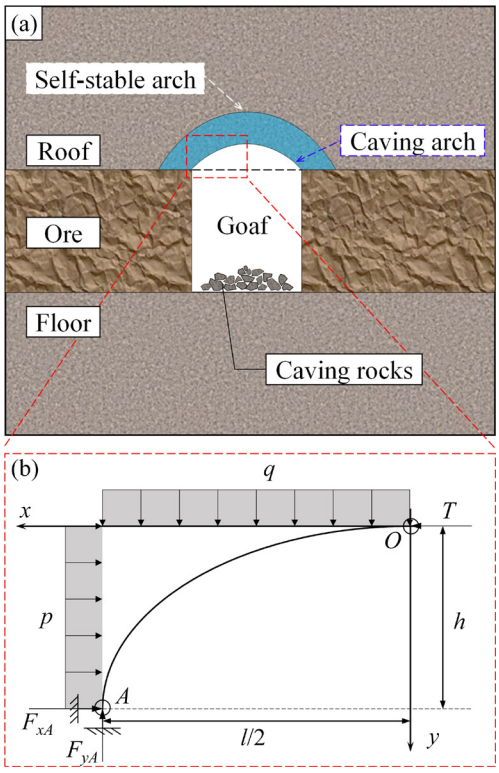

Fig. 2 Mechanical model of roof in one-step mining: (a) Schematic diagram of room-stope mining; (b) Arch mechanical model

Figure 2(b) shows a simplified mechanical diagram of caving arch, where F_{xA} is the horizontal support reaction force of Point A, F_{yA} is the vertical support reaction force of Point A, T is the horizontal support reaction force of the vault, q is the vertical load, p is the horizontal load, h is the height of caving area, and l is the width of goaf. Based on the symmetry of the arch, the left side is taken for mechanical analysis. After the collapse of the roof, the rock fissures are developed and cannot provide rotational restraint, so it is simplified to be hinged at the vault and arch. According to the structural mechanics static equilibrium condition, the caving arch satisfies Eq. (1):

$$\sum F_x=0,\ \sum F_y=0,\ \sum M_O=0 \tag{1}$$

where $\sum F_x$ is the horizontal resultant force, $\sum F_y$ is the resultant force in the vertical direction, and $\sum M_O$ is the bending moment at point O.

Natural arch maintains static balance in the form of a pressure arch, so the direction of the maximum principal stress in the arch should coincide with the track of the arch axis, the bending moment at any point in the arch is zero, and Eq. (2) is satisfied

$$\sum M_x=0 \tag{2}$$

where $\sum M_x$ is the bending moment at any point in the arch.

Combining Eqs. (1) and (2), the equation of the arch axis $y=f(x)$ can be solved as shown in Eq. (3):

$$f(x)=\frac{ql^2+4ph^2}{8ph}-\sqrt{\left(\frac{ql^2+4ph^2}{8ph}\right)^2-\frac{qx^2}{p}} \tag{3}$$

During the two-step mining, the room-stope has been filled. The backfill is in contact with the roof and provides radial stress, the roof changes from uniaxial stress state to triaxial stress state, and the stability is enhanced. The stress state of the roof, which is not in contact with the backfill, has also changed. It shows that the arch foot support point rises from Point A to Point N, the width of the goaf decreases from l to l', and the height of the caving area decreases from h to h', as shown in Fig. 3. At this time, the ratio between the contact arc length ($l_{\widehat{NA}}$) of the backfill and the roof to the initial arc length ($l_{\widehat{OA}}$) of the caving arch can be used to express the RCFR (η), satisfying Eq. (4):

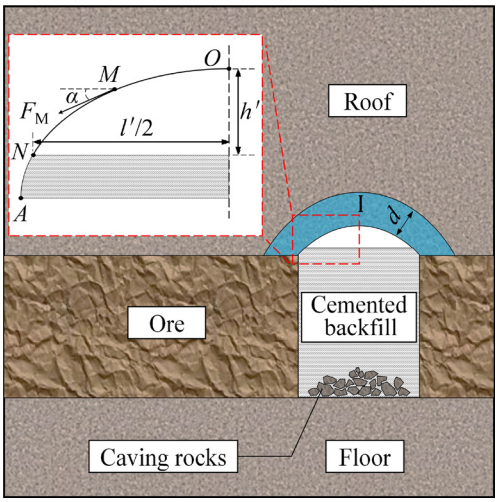

Fig. 3 Diagram of filling of room-stope

$$\eta = l_{\widehat{NA}}/l_{\widehat{OA}} = \left[\int_{l'/2}^{l/2}\sqrt{1+f'^2(x)}\ \mathrm{d}x\right] \Big/ \left[\int_{0}^{l/2}\sqrt{1+f'^2(x)}\ \mathrm{d}x\right] \tag{4}$$

Because the integral solution process of Eq. (4) is complex, the solution is simplified, the relationship between l' and η approximately satisfies Eq. (5), and the relationship between h' and η satisfies Eq. (6):

$$l' = g_1(\eta) \approx (1-\eta)l \tag{5}$$

$$h' = g_2(\eta) \approx (1-\eta)h \tag{6}$$

From Eq. (1), the relevant variables F_{xM}, F_{yM} and α of the axial force (F_M) at any position on Section $\widehat{ON}$ where the cemented backfill is not in contact with the roof can be found to satisfy Eqs. (7) to (9), respectively.

$$F_{xM} = \frac{ql'^2 + 4ph'^2}{8h'} - py \tag{7}$$

$$F_{yM} = qx \tag{8}$$

$$\tan\alpha = F_{yM}/F_{xM} \tag{9}$$

where F_{xM} is the horizontal component of F_M, F_{yM} is the vertical component of F_M, and α is the angle between the F_M and the horizontal direction.

According to Eq. (3), the equation of the arch axis of the roof after filling can be found, and combination with Eqs. (5) to (8), the axial force (F_I) at point M can be expressed as

$$F_I = \sqrt{\left[\frac{qg_1^2(\eta)+4pg_2^2(\eta)}{8g_2(\eta)}\right]^2 + q(q-p)x^2} \tag{10}$$

Since $g_1(\eta)$ and $g_2(\eta)$ are both decreasing functions, it is clear from Eq. (10) that the axial force within Rock Arch I declines continuously as the value of η increases. As the vertical load is greater than the horizontal load, the maximum axial force occurs at point N of the arch foot when the value of η is constant. Conversely, the maximum axial force occurs at Point O of the vault. When the maximum axial force (F_{max}) in Rock Arch I is less than the compressive strength of the rock mass, it can be considered that the roof of goaf is in a stable state. At this time, the F_{max} satisfies Eq. (11):

$$F_{max}/d \le [\sigma_c] \tag{11}$$

where $[\sigma_c]$ is the compressive strength of the roof rock, and d is the thickness of the rock arch. As per the nature arch theory, the thickness of the rock arch is the same as the height of the caving arch [36].

3.2 Self-stable arch model of roof in two-step mining

During the second step mining, as the RCFR is low in one-step mining, as shown in Fig. 4, the self-stable balance arch of the room-stope will lose its support in Area II_1, and the backfill cannot provide support in Area II_2 to ensure the formation of self-stable balance arch at the roof of pillar-stope. Therefore, the cracks in the roof will continue to expand inward, resulting in a large amount of rock mass caving and further large-scale roof instability. In order to render the backfill to provide support in Area II_2, the η should satisfy Eq. (12):

$$\int_{g_1(\eta)}^{l} \mathrm{d}s \ge d \tag{12}$$

where ds is the arc differential.

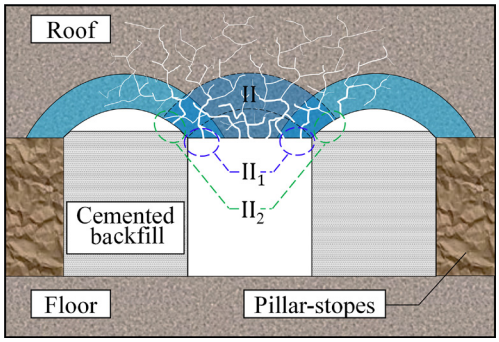

Fig. 4 Roof instability state diagram in two-step mining

As the RCFR is high in one-step mining, as shown in Fig. 5(a), after the pillar-stope is mined, the cracks in the surrounding rock of the roof expand inward, and a small amount of rock falls,

but the backfill on both sides can provide effective support in Area III_2. Therefore, it is possible to form a self-stable balance arch in Area II, which prevents further inward expansion of the cracks. At the same time, Rock Arch II can also provide support for Rock Arch I in Area III_1, ensuring the overall stability of the roof in the mines. The load bearing of Rock Arch II is shown in Fig. 5(b). It bears the vertical load q in Section $\widehat{OR}$ and the axial force F_N applied by the arch foot of Rock Arch I in Section $\widehat{RB}$. Compared with the load bearing condition of Rock Arch I in Fig. 2(b), both sides of Rock Arch II are backfilling. At this time, the stress in the horizontal direction has been released, but an axial force exerted by Rock Arch I is added.

From Eqs. (1) and (10), the axial force (F_{II}) within Rock Arch II can be solved to satisfy Eq. (13). It can be seen that the RCFR of the backfill on both sides directly affects the stress state of the roof during subsequent excavation. Moreover, the axial force F_{II} is a segmental function, and the stress state abruptly changes near Point R.

$$F_{II}=\begin{cases}\left\{\left[\dfrac{ql^2}{8h}+\dfrac{qg_1^2(\eta)-4pg_2^2(\eta)}{16g_2(\eta)}\cos\alpha+\right.\right.\\ \left.\left.qg_1(\eta)\sin\alpha\right]^2+q^2x^2\right\}^{1/2},\\ x\in\left(0,\ \dfrac{l}{2}-h\sin\alpha\right)\\ \left\{\left[\dfrac{ql^2}{8h}+\dfrac{qg_1^2(\eta)-4pg_2^2(\eta)}{8g_2(\eta)}\right.\right.\\ \left.\left(\dfrac{\cos\alpha}{2}-\dfrac{2x+2h\sin\alpha-l}{2h\sin\alpha}\right)+\right.\\ \left.qg_1(\eta)\sin\alpha\right]^2+\\ \left.\left(qg_1(\eta)\dfrac{2x+2h\sin\alpha-l}{2h\sin\alpha}\right)^2\right\}^{1/2},\\ x\in\left(\dfrac{l}{2}-h\sin\alpha,\ \dfrac{l}{2}\right)\end{cases}\tag{13}$$

3.3 Optimization of roof-contacted filling rate

The room-stope and pillar-stope in the Dongguashan Copper Mine are arranged at intervals, and the width (l) of all stopes is 18 m. As per the natural arch theory, the height (h) of the caving area under the condition of no support satisfies Eq. (14):

$$h=l/(2f_k)\tag{14}$$

where f_k is the firmness coefficient of the roof rock mass, which is taken as 1/10 of the uniaxial compressive strength.

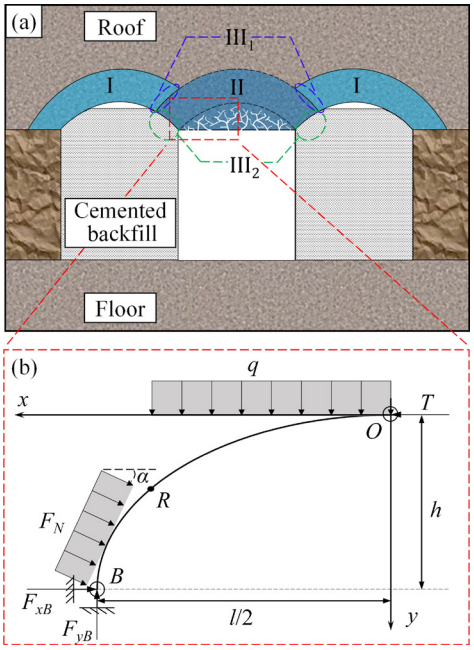

Fig. 5 Mechanical model of roof in two-step mining: (a) Schematic diagram of pillar-stope mining; (b) Arch mechanical model

The stope height changes with the thickness of the ore body. In this study, the effect of RCFR on roof stability was analyzed, taking the stope with a height of 25 m as an example. According to the measured data of the in-situ stress field of the mines, the direction of the maximum principal stress was consistent with the trend of the ore body, taking 32.75 MPa. The intermediate principal stress was in the vertical direction, taking 12.23 MPa. The minimum principal stress was perpendicular to the trend of the ore body, taking 8.69 MPa. The rock core was drilled from the site and processed into standard samples for uniaxial compression. The uniaxial compressive strength of the roof rock sample was determined to be 57.31 MPa. However, discontinuous surfaces such as joints and fissures within the rock mass weakened the strength of the rock. In practical engineering applications, the strength of the rock mass needs to be reduced using the Hoek−Brown criterion [37]. Finally, Eq. (15) was used to determine the uniaxial compressive strength of the roof rock mass as 10.82 MPa.

$$\begin{cases}\sigma_1=\sigma_3+\sqrt{m_b\sigma_3\sigma_c+s\sigma_c^2}\\ \sigma_t=\dfrac{\sigma_c}{2}\left(m_b-\sqrt{m_b^2+4s}\right)\\ m_b=m_i\exp[(f_{GSI}-100)/28]\\ s=\exp[(f_{GSI}-100)/9]\end{cases}\tag{15}$$

where σ_1 is the uniaxial compressive strength of rock mass, σ_c is the uniaxial compressive strength of standard rock sample, σ_t is the uniaxial tensile strength of rock mass, m_b, m_i and s are Hoek−Brown parameters, m_i is the Hoek−Brown constant of intact rock, and the value of roof rock mass is 9, f_{GSI} is the geological strength index, and the value of roof rock mass is 70.

The risk of roof instability is higher in two-step mining compared to one-step mining. From Eq. (12), it can be obtained that when η<67%, the backfill was difficult to provide effective support to Rock Arch II due to insufficient contact with it, which would cause a large-scale collapse of the roof. The stress state of Rock Arch II for five values of η was calculated according to Eq. (13) and the results are shown in Fig. 6. It was revealed that the stress state in Rock Arch II was divided into two stages. In the first stage, the stress increased from the vault to Point R, and in the second stage, the stress decreased slowly from Point R to the arch foot. The stress state reached the maximum at Point R and changed suddenly, which was the intersection of Rock Arch I and Rock Arch II. With the increase in RCFR, the stress in most areas of the arch decreased, and Point R moved towards the arch foot. When the η<75% in the room-stope, with the gradual caving of the roof rock in the pillar-stope, the stress state of the roof was redistributed. The stress everywhere in the Rock Arch II would gradually increase and eventually exceed its uniaxial compressive strength. Therefore, it needs to be filled and fully connected to the roof in time to make the roof completely in the triaxial stress state, which will ensure the stability of the roof. However, when the capping rate of the one-step quarry filling reached 80%, the stress in the rock body within 2.7 m from the vault was less than its own uniaxial compressive strength and was in a self-stable state for a long time. At this time, it was sufficient for the RCFR in pillar-stope to reach 70%. In the actual production process, the RCFR in each stope was essentially the same. After calculation, when the RCFR of each stope reached 77%, the stress in the area which was not in contact with the backfill in Rock Arch II was less than its own uniaxial compressive strength, so as to ensure the long-term stability of the goaf.

In order to study the stress state of pillar-stope roof under different in-situ stress environments, it was assumed that the RCFR of room-stope was 80%. Figure 7(a) shows the effect of vertical stress on the stress state of rock Arch II when the horizontal stress is 8 MPa. It was illustrated that the

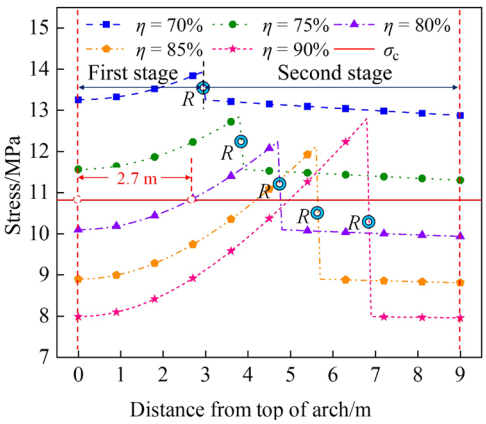

Fig. 6 Stress distribution on roof of pillar-stope at different roof-contacted filling rates

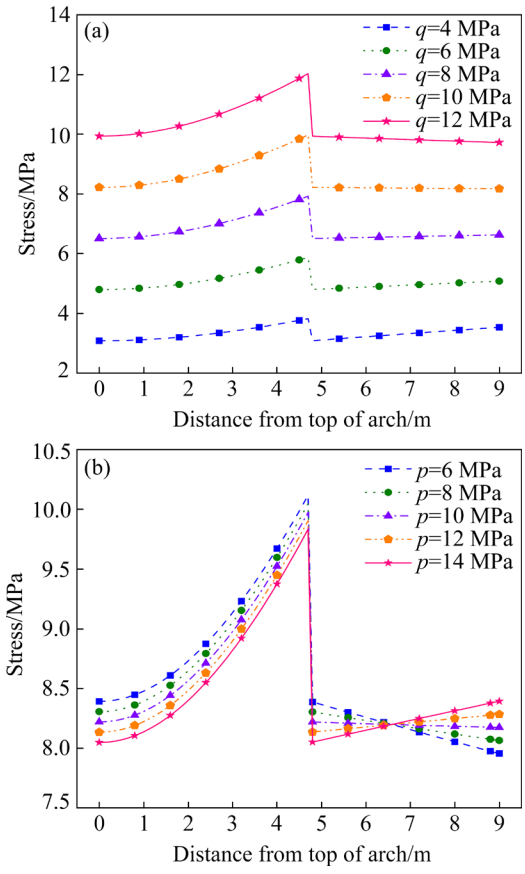

Fig. 7 Stress distribution on roof of pillar-stope at different in-situ stresses: (a) p=8 MPa; (b) q=10 MPa

stress of Rock Arch II increased with the increase of vertical stress, but the overall curve trend was similar. The results of previous studies indicated that when $q>p$, the stress at the arch foot of Rock Arch I was the highest. When $q<p$, the stress at the vault was the highest. However, the position of the highest stress of the roof was independent of vertical stress in the two-step mining, but was only affected by the RCFR in room-stope, which always occurs at 4.7 m away from the vault. As shown in Fig. 7(b), when the vertical stress was 10 MPa, with increasing the horizontal stress, only the stress in a small part of the arch foot increased, while the stress in most other areas declined slightly. This was because the stope completed by one-step mining formed a goaf during two-step mining, which isolated the transmission of horizontal stress and made the horizontal stress not act on the pillar-stope. Therefore, horizontal stress had little impact on two-step mining.

4 Numerical simulation and engineering verification

4.1 Numerical simulation

The mine numerical model was established by using particle flow code (PFC) software to study the deformation characteristics of roof in the process of stope mining and filling. In PFC2D model, rock material is composed of a large number of circular particles, and the force between particles is called contact. A variety of contact models are built in PFC2D model. Among them, the parallel linear contact model can not only provide the elastic force between particles, but also have a parallel bond. After the parallel bond is generated, it can resist the shear and tensile force between particles, which is suitable for simulating rock materials. The macroscopic deformation and failure characteristics of rock are determined by the input microscopic parameters. Firstly, the rock parameters of the roof should be calibrated by a uniaxial compression test. By adjusting the microcosmic parameters, the numerical simulation results exhibit the identical macroscopic failure characteristics as the experimental findings. As shown in Fig. 8, the errors of uniaxial compressive strength and Young's modulus by parameter calibration were not more than 1%. It was worth noting that the difference in peak strain did not affect the subsequent simulation results. This was because there were natural fractures in the real rock, leading to certain deformation of the rock in the initial stage of compression, while for the numerical model consisting of a compacted assembly of rigid particles, there was no fracture compaction stage [38]. Then, the parameters of other rocks were calibrated by the same method. Finally, the calibrated micro parameters were reduced according to the Hoek−Brown criterion to obtain the micro parameters of different rock masses, as shown in Table 1.

According to the stope with a width of 18 m, the size of the mine numerical model was 168 m × 168 m to ensure that the boundary rock mass was still in the original rock stress state during stope mining. Theoretically, the smaller the particle radius is and the greater the number of particles is, and the more accurate the simulation results are; but an increase in the number of particles will in turn exponentially reduce the efficiency of the calculation. Therefore, a small radius range of 0.2−0.4 m was used to randomly generate particles

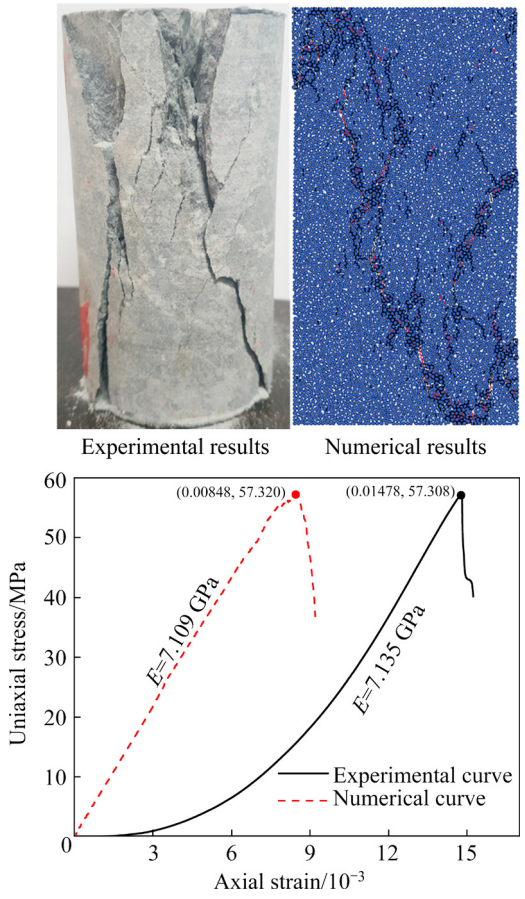

Fig. 8 Comparison between numerical simulation results and experimental results under uniaxial compression

Table 1 Microscopic parameters of different rock masses

Specimen	ρ/(kg·m^{-3})	E/GPa	$\bar{E}_c$/GPa	c/ MPa	φ/ (°)	$\bar{\sigma}_t$ /MPa	υ	μ	k_n/k_s	$\bar{k}_n/\bar{k}_s$
Ores	3220	34.35	34.35	8.86	45.1	3.04	0.312	0.5	2.0	2.0
Roof rock	2700	4.71	4.71	3.84	35.6	1.7	0.329	0.5	2.0	2.0
Floor rock	2720	14.87	14.87	6.60	45.9	2.24	0.209	0.5	2.0	2.0
Cemented backfill	1740	0.97	0.97	0.96	33.0	0.40	0.200	0.5	2.0	2.0
Uncemented backfill	1740	0.57	0.57	–	–	–	0.100	0.5	2.0	2.0

ρ is the particle density, E is the effective modulus, $\bar{E}_c$ is the parallel-bond effective modulus, c is the cohesion, φ is the internal friction angle, $\bar{\sigma}_t$ is the tensile strength, υ is the Poisson ratio, μ is the friction coefficient, k_n/k_s is the particle stiffness ratio, $\bar{k}_n/\bar{k}_s$ is the parallel-bond stiffness ratio.

in the excavation area in the middle of the model. The particle radius gradually increased from the excavation area to the model boundary, and increased to about 2 m at the model boundary. A total of 24992 particles were generated in this model, as shown in Fig. 9. According to the measured in-situ stress state of the mines, the stress of 8.69 MPa was applied to the horizontal boundary and 12.23 MPa was applied to the vertical boundary of the model, and the vertical downward gravity acceleration (g) was applied to the particles to simulate the gravity environment. Then, room-stope 1 (RS-1), room-stope 2 (RS-2) and pillar-stope 1 (PS-1) were mined in turn, and the stability of the roof in the mining process was observed.

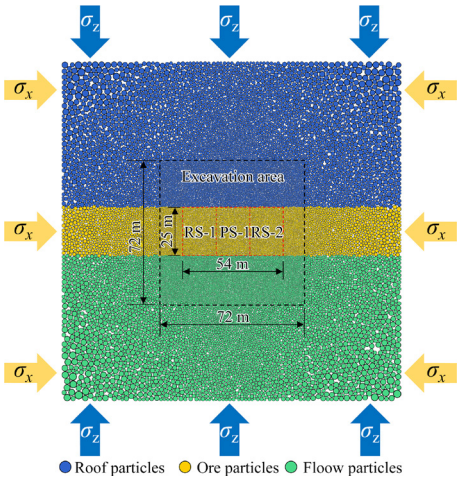

Fig. 9 Numerical model of mine

The first step was to mine RS-1. After trial calculation, it was found that the height of the caving area was about 7 m, which was close to the calculation results. Therefore, three monitoring points were placed at 7 m above the roof, from the left to the right, Monitoring Points 1 (MP-1), 2 (MP-2) and 3(MP-3), to monitor the displacement of the roof in the non-caving area. A total of 5×10^5 cycles were calculated. The vertical displacement of the three monitoring points is shown in Fig. 10. Figures 10(a−d) show the roof state when calculating 0, 1×10^5, 3×10^5 and 5×10^5 cycles, respectively. It was indicated that after RS-1 excavation, two large rock masses of the roof fell successively, and then the roof remained stable. The shape of the caving area was roughly an arch structure. The displacement change trend of the three monitoring points was roughly the same, and the displacement on the right side of the roof was slightly larger than that on the left. The roof displacement increased rapidly after RS-1 excavation. The vertical displacement of MP-2 in the middle of the roof increased to 9 mm and gradually remained stable. Then, at 1.5×10^5 cycles, there was a slight vibration on the roof, resulting in a small amount of rebound and then gradually sinking at a slow speed. Further analysis revealed that the vibration of the roof was a microseismic phenomenon caused by the collision between the falling stones and the floor. On the whole, the roof was in a stable state before the vibration, and the roof displacement tended to increase after the vibration, but the growth rate was slow and the overall displacement was small. The roof was in a tentative stable state as a whole, but its stability was easily affected by dynamic signals such as mechanical vibration in the subsequent mining process, so it needed to be filled in time.

Theoretical studies have demonstrated that when the RCFR was low, the roof would be unstable over a large area. To ensure the stability of the roof during the subsequent recovery process, it was recommended that the RCFR value was greater than 77%. Therefore, in this simulation three roof-contacted filling rates of 20%, 80% and

100% were selected to verify the theoretical results. Figure 11 presents the roof deformation evolution process at different time during the mining and filling simulation of the three stopes. After RS-2 mining, the roof rock mass at the upper part of the stope fell, forming the identical arch self-stable structure. However, owing to the redistribution of underground space stress caused by mining, the

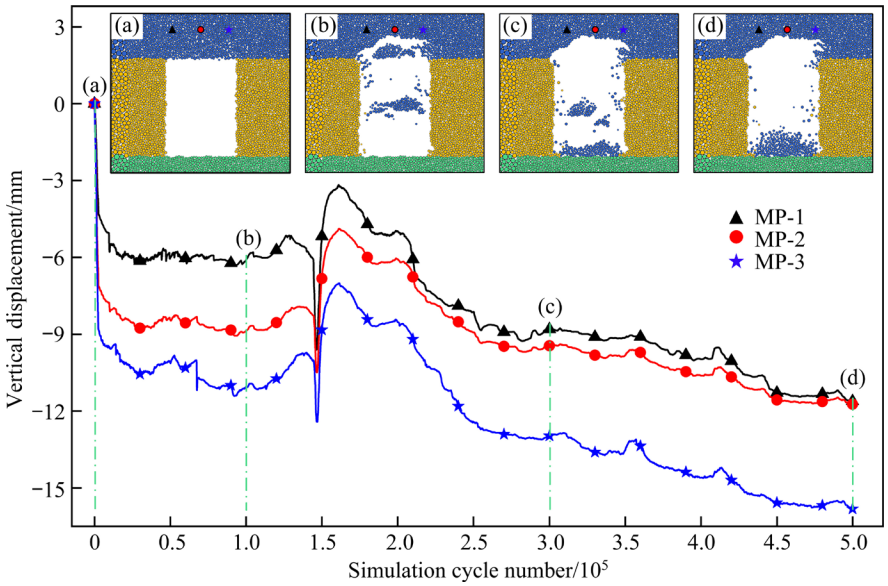

Fig. 10 Variation of vertical displacement of roof during RS-1 mining: (a) 0 cycle; (b) 1×10^5 cycles; (c) 3×10^5 cycles; (d) 5×10^5 cycles

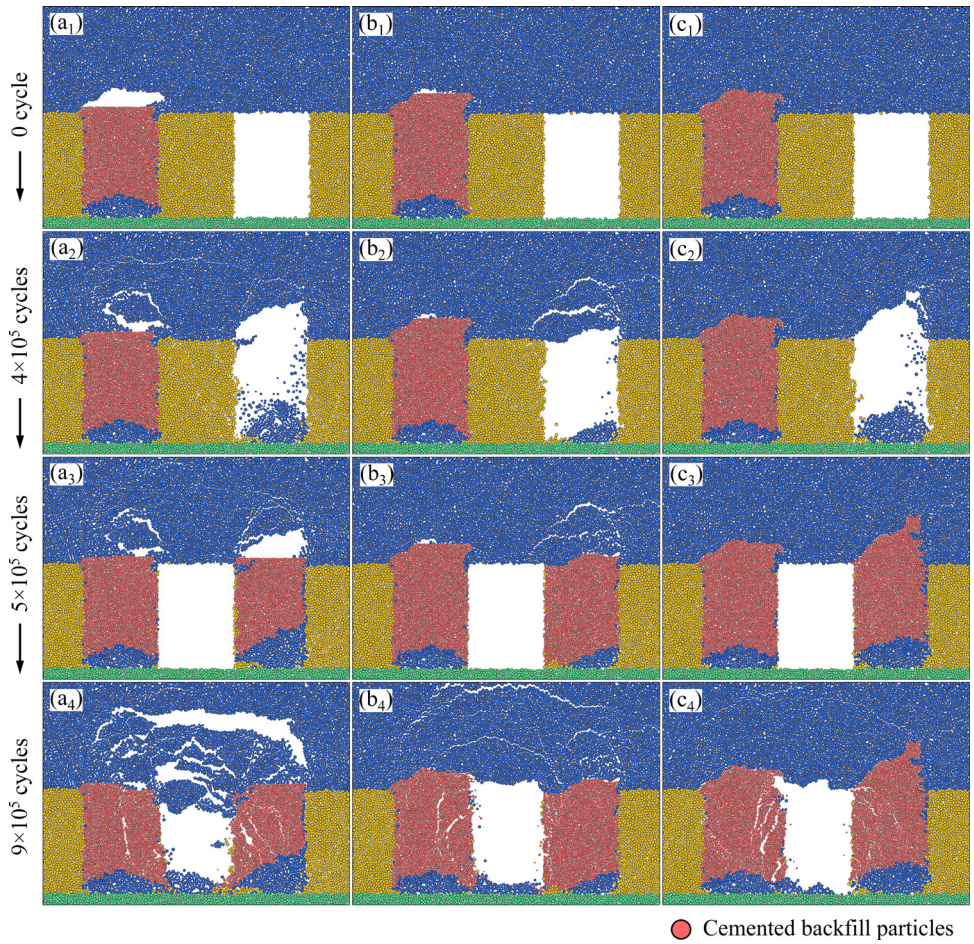

Fig. 11 Roof deformation evolution process at different RCFR values: (a) η=20%; (b) η=80%; (c) η=100%

RS-1 roof with a RCFR of 20% experienced secondary caving, forming a larger arch shaped zone, as shown in Fig. 11(a_2). However, when the RCFR values were 80% and 100%, there was no evident deformation of the RS-1 roof under the effective support of the backfill, as shown in Figs. 11(b_2) and (c_2), respectively. After PS-1 mining, the backfills on both sides with a RCFR of 20% did not provide effective support, resulting in a large area of roof collapse. Although a large self-stable balance arch within the width of three stopes was formed, as shown in Fig. 11(a_4), too many caving rocks seriously affected the goaf filling and subsequent mining. When the RCFR values were 80% and 100%, a certain settlement occurred in the surrounding rock of the roof, and the backfills on both sides were split, as shown in Figs. 11(b_4) and 11(c_4), respectively. However, there was no large-area caving and overall instability of roof, which ensured the smooth progress of subsequent filling work. It can also be seen from Fig. 11(b_4) that the crack formed an arch curve in the PS-1 roof, and the arch foot acted completely on the backfills on both sides, which verified the arch bearing structure proposed by the theoretical model.

Finally, PS-1 with full tailings was filled as compared to the filling effect when the RCFR was 80% and 100%, as shown in Fig. 12. After filling the goaf at 80% RCFR for a period of time, the roof slowly sank and then remained stable after full contact with the backfill, while the roof settled insignificantly at 100% RCFR. The Monitoring Point 4 (MP-4) was arranged on the roof to monitor the displacement variation in the roof, as shown in Fig. 12(a). The monitoring results showed that the roof still moved downward after the filling was

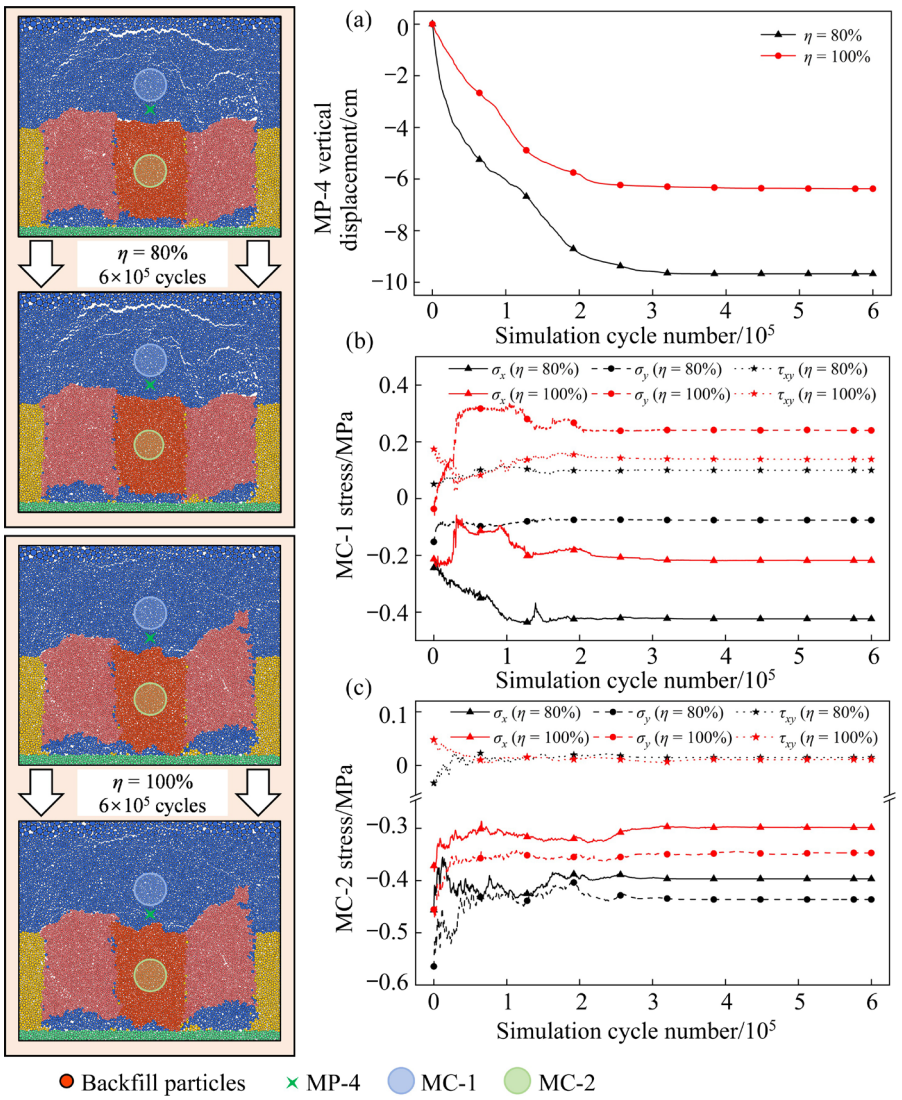

Fig. 12 Displacement and stress variation after PS-1 filling: (a) Results of vertical displacement monitoring; (b) Results of roof stress monitoring; (c) Results of backfill stress monitoring

completed. The roof of the goaf with 100% RCFR retained stability first, and the final vertical displacement was about 6 cm, while the roof of the goaf with 80% RCFR continued to sink, and retained stability when the displacement reached about 10 cm. Measurement circles 1 (MC-1) and 2 (MC-2) were arranged in the roof and backfill, respectively, to monitor the stress changes in the roof and backfill after filling, as shown in Figs. 12(b) and (c). With the settlement of the roof, the stress state of the roof and the backfill changed continuously, but it remained constant in the end. The horizontal stress (σ_x) in the roof was greater than the vertical stress (σ_y) in both RCFR cases, and the shear stress (τ_{xy}) was relatively small. Compared with 100% RCFR, the horizontal stress of the roof at 80% RCFR was greater, but the vertical stress was smaller. The stress state in the backfill was that the vertical stress was greater than the horizontal stress, and there was almost no shear stress. The horizontal and vertical stresses of the backfill at the RCFR value of 80% were greater than those at the RCFR value of 100%. On the whole, the horizontal stress was mainly in the middle of the roof, which was the same as the conclusion that the axial force in the middle of the arch structure was in the horizontal direction. The higher the filling roof connection rate is, the smaller the roof deformation is, the smaller the stress between the roof and the filling body is, and the higher the stability of the stope is. Overall, the middle of the roof was dominated by horizontal stress, which was additionally identical to the middle of the arch structure. The higher the RCFR is, the lower the deformation of the roof is, the lower the stress within the roof and backfill is, and the higher the stability of the stope is. The increase in RCFR reduced the deformation of the roof, diminished the stress in the roof and backfill, and improved the stability of the stope.

4.2 Field engineering verification

In order to detect the real roof caving and deformation after the actual mining in the Dongguashan mining area, the 3D cavity monitoring system (CMS) developed by Optech Company was used to scan the goaf [33], and the scanning data were processed by using the Qvol software equipped with CMS, and then the 3D model of goaf was established by using digital mine modeling software. The scanning results of goaf are shown in Fig. 13.

Figures 13(a) and (b) present the scanned views of the mining area on exploration Lines 50 and 52, respectively, which included a 3D scanned top view and a section of the middle of the goaf. The room-stope and pillar-stope were arranged alternately, and the room-stope was slightly longer than the pillar-stope. There was good control over the mining of each stope, with no over-excavation or under-excavation. Seen from the section of goaf, only the roof of Stopes 50-13 and 52-11 was relatively flat without obvious caving, while the roof of other stopes was arc-shaped. After mining, each goaf was filled in accordance with the design requirements of 80% RCFR, and the on-site construction error did not exceed 10%. ZLGH−20 borehole stress gauges and BGK−A3 multi-point displacement gauges were installed on the roof of Stopes 50-15 and 52-09 to monitor the changes in stress and displacement of the roofs. After 6 months of monitoring, the stability of the goaf roof after filling was good, and there was no secondary caving. The roof monitoring results indicated that the maximum stress of Stope 50-15 was 0.57 MPa and the maximum displacement was 7.16 cm, while the maximum stress of Stope 52-09 was 0.72 MPa and the maximum displacement was 8.91 cm. The backfill had an obvious supporting effect on the roof, and the roof stress and displacement were within the safe range, which was close to the theoretical and numerical simulation results, verifying the reasonableness of the theoretical analysis.

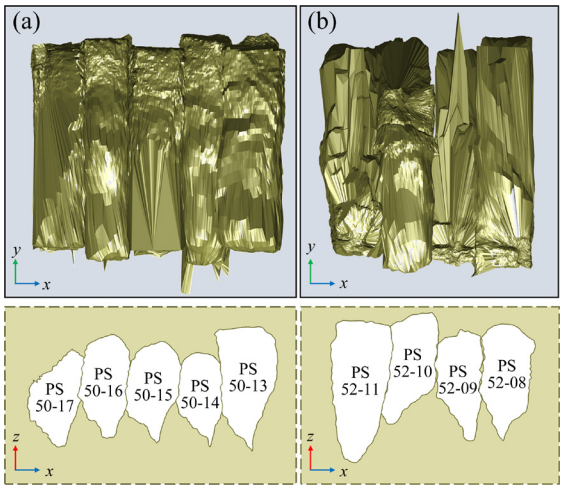

Fig. 13 Scan results of goaf at exploration Lines 50 (a) and 52 (b)

5 Conclusions

(1) When the vertical stress was greater than the horizontal stress, the maximum stress of the roof in room-stope appeared at the arch foot, on the contrary, the maximum stress occurred at the vault. The roof stress of the pillar-stope was less influenced by horizontal stress, but increased remarkably with the vertical stress.

(2) When the RCFR of the room-stope was less than 67%, the roof of the pillar-stope was difficult to form a self-stable balance arch. In the continuous mining process with the same RCFR in each stope, the higher the RCFR is, the better the stope stability is. When the RCFR was lower than 77%, there was a risk of roof instability due to exceeding the bearing capacity of the rock arch.

(3) The numerical simulation results revealed that the roof was dominated by horizontal stress. When the RCFR reached 80%, the arch effect of the roof was obvious. The field monitoring data were close to the theoretical analysis and numerical simulation findings, which fully verified the reasonableness of the theoretical analysis.

Acknowledgments

The work was supported by the National Natural Science Foundation of China (Nos. 12072376, 52174140), and the Fundamental Research Funds for Central Universities of the Central South University, China (No. 2020zzts195).

References

[1] MA Shao-wei, HU Jian-hua, QIU Ya-guang, REN Qi-fan, YANG Dong-jie. Bearing mechanism and thickness optimization of ore roof in bauxite stope [J]. Transactions of Nonferrous Metals Society of China, 2022, 32(1): 285−295.

[2] MA Hai-tao, WANG Ji-nan, WANG Yun-hai. Study on mechanics and domino effect of large-scale goaf cave-in [J]. Safety Science, 2012, 50(4): 689−694.

[3] LI Xi-bing, QIU Jia-dong, ZHAO Yu-zhe, CHEN Zheng-hong, LI Di-yuan. Instantaneous and long-term deformation characteristics of deep room-pillar system induced by pillar recovery [J]. Transactions of Nonferrous Metals Society of China, 2020, 30(10): 2775−2791.

[4] KUANG Tie-jun, LI Zhu, ZHU Wei-bing, XIE Jian-lin, JU Jin-feng, LIU Jin-rong, XU Jing-min. The impact of key strata movement on ground pressure behaviour in the Datong coalfield [J]. International Journal of Rock Mechanics and Mining Sciences, 2019, 119: 193−204.

[5] YU Bin, GAO Rui, KUANG Tie-jun, HUO Bing-jie, MENG Xiang-bin. Engineering study on fracturing high-level hard rock strata by ground hydraulic action [J]. Tunnelling and Underground Space Technology, 2019, 86: 156−164.

[6] LI Chun-yuan, ZUO Jian-ping, SHI Yue, WEI Chun-chen, DUAN Yu-qing, ZHANG Yong, YU Hong. Deformation and fracture at floor area and the correlation with main roof breakage in deep longwall mining [J]. Natural Hazards, 2021, 107(2): 1731−1755.

[7] WANG Shu-ren, WU Xiao-gang, ZHAO Yan-hai, HAGAN P. Mechanical performances of pressure arch in thick bedrock during shallow coal mining [J]. Geofluids, 2018, 2018: 1−13.

[8] ZHU Cheng, YUAN Yong, YUAN Chao-feng, LIU Fu-quan, CHEN Zhong-shun, WANG Sheng-zhi. Study on the structural forms of the key strata in the overburden of a stope during periodic weighting and the reasonable working resistance of the support [J]. Energy Science & Engineering, 2020, 8(7): 2599−2620.

[9] YUAN Yong, TU Shi-hao, ZHANG Xiao-gang, LI Bo. Dynamic effect and control of key strata break of immediate roof in fully mechanized mining with large mining height [J]. Shock and Vibration, 2015, 2015: 657818.

[10] TAO Zhi-gang, SONG Zhi-gang, HE Man-chao, MENG Zhi-gang, PANG Shi-hui. Principles of the roof cut short-arm beam mining method (110 method) and its mining-induced stress distribution [J]. International Journal of Mining Science and Technology, 2018, 28(3): 391−396.

[11] YAO Bang-hua, WANG Deng-ke, WANG Yun-gang, WEI Jian-ping. Mechanical mechanism study on the effect of fully-mechanized mining with filling on key strata deformation [J]. Disaster Advances, 2013, 6: 196−203.

[12] XIA Bin-wei, JIA Jin-long, YU Bin, ZHANG Xuan, LI Xiao-long. Coupling effects of coal pillars of thick coal seams in large-space stopes and hard stratum on mine pressure [J]. International Journal of Mining Science and Technology, 2017, 27(6): 965−972.

[13] HAN Hong-kai, XU Jia-lin, WANG Xiao-zhen, XIE Jian-lin, XING Yan-tuan. Method to calculate working surface abutment pressure based on key strata theory [J]. Advances in Civil Engineering, 2019, 2019: 7678327.

[14] WEN Zhi-jie, XING En-rui, SHI Shao-shuai, JIANG Yu-jing. Overlying strata structural modeling and support applicability analysis for large mining-height stopes [J]. Journal of Loss Prevention in the Process Industries, 2019, 57: 94−100.

[15] CUI Xi-min, GAO Yong-ge, YUAN De-bao. Sudden surface collapse disasters caused by shallow partial mining in Datong coalfield, China [J]. Natural Hazards, 2014, 74(2): 911−929.

[16] CHEN Tuo, MITRI H S. Strategies for surface crown pillar design using numerical modelling — A case study [J]. International Journal of Rock Mechanics and Mining Sciences, 2021, 138(12): 104599.

[17] KUMAR H, DEB D, CHAKRAVARTY D. Design of crown pillar thickness using finite element method and multivariate regression analysis [J]. International Journal of Mining Science and Technology, 2017, 27(6): 955−964.

[18] LI Peng, CAI Mei-feng. Challenges and new insights for exploitation of deep underground metal mineral resources [J]. Transactions of Nonferrous Metals Society of China, 2021, 31(11): 3478−3505.

[19] CUI Feng, LEI Zhao-yuan, CHEN Jian-qiang, CHANG Bo, YANG Yan-bin, LI Chang-lu, JIA Chong. Research on

reducing mining-induced disasters by filling in steeply inclined thick coal seams [J]. Sustainability, 2019, 11(20): 5802.
[20] TAO Ming, CHENG Wen-qing, NIE Ke-mi, ZHANG Xu, CAO Wen-zhuo. Life cycle assessment of underground coal mining in China [J]. Science of the Total Environment, 2022, 805: 150231.
[21] SHANG De-lei, YIN Guang-zhi, LI Xiao-shuang, LI Yao-ji, JIANG Chang-bao, KANG Xiang-tao, LIU Chao, ZHANG Chi. Analysis for green mine (phosphate) performance of China: An evaluation index system [J]. Resources Policy, 2015, 46: 71−84.
[22] TAO Ming, ZHANG Xu, WANG Shao-feng, CAO Wen-zhuo, JIANG Yi. Life cycle assessment on lead–zinc ore mining and beneficiation in China [J]. Journal of Cleaner Production, 2019, 237: 117833.
[23] FAN Bo, ZHAO Long-sheng, FENG Zong-yu, LIU De-peng, YIN Wei-qiang, LONG Zhi-qi, HUANG Xiao-wei. Leaching behaviors of calcium and magnesium in ion-adsorption rare earth tailings with magnesium sulfate [J]. Transactions of Nonferrous Metals Society of China, 2021, 31(1): 288−296.
[24] WANG Hong-wei, POULSEN B A, SHEN Bao-tang, XUE Sheng, JIANG Yao-dong. The influence of roadway backfill on the coal pillar strength by numerical investigation [J]. International Journal of Rock Mechanics and Mining Sciences, 2011, 48(3): 443−450.
[25] HOU Chen, ZHU Wan-cheng, YAN Bao-xu, GUAN Kai, NIU Lei-lei. Analytical and experimental study of cemented backfill and pillar interactions [J]. International Journal of Geomechanics, 2019, 19(8): 04019080.
[26] TESARIK D R, SEYMOUR J B, YANSKE T R. Long-term stability of a backfilled room-and-pillar test section at the Buick Mine, Missouri, USA [J]. International Journal of Rock Mechanics and Mining Sciences, 2009, 46(7): 1182−1196.
[27] TAN Yu-yue, ZHANG Kai, YU Xin, SONG Wei-dong, WANG Jie, HAI Cheng-long. The mechanical and microstructural properties of composite structures made of a cement-tailing backfill and rock core [J]. Minerals, 2020, 10(2): 159.
[28] KOSTECKI T, SPEARING A J S. Influence of backfill on coal pillar strength and floor bearing capacity in weak floor conditions in the Illinois Basin [J]. International Journal of Rock Mechanics and Mining Sciences, 2015, 76: 55−67.
[29] ZHU Xiao-jun, GUO Guang-li, FANG Qi. Coupled discrete element–finite difference method for analyzing subsidence control in fully mechanized solid backfilling mining [J]. Environmental Earth Sciences, 2016, 75(8): 683.
[30] FENG Xiao-jun, ZHANG Qi-ming, ALI M. 3D modelling of the strength effect of backfill-rocks on controlling rockburst risk: A case study [J]. Arabian Journal of Geosciences, 2020, 13(3): 1−16.
[31] ZHOU Nan, ZHANG Ji-xiong, YAN Hao, LI Meng. Deformation behavior of hard roofs in solid backfill coal mining using physical models [J]. Energies, 2017, 10(4): 557.
[32] JIANG Li-chun, CHEN Peng, WU Ai-xiang. Roof self-stabilizing arching effect of goaf based on different roof-contacted filling rate [J]. The Chinese Journal of Nonferrous Metals, 2019, 29(1): 187−193. (in Chinese)
[33] HUANG Zhi-guo, DAI Xing-guo, DONG Long-jun. Buckling failures of reserved thin pillars under the combined action of in-plane and lateral hydrostatic compressive forces [J]. Computers and Geotechnics, 2017, 87: 128−138.
[34] WANG Feng, CHEN Shao-jie, XU Jia-lin, REN Meng-zi. New method to design coal pillar for lateral roof roadway based on mining-induced stress: A case study [J]. Advances in Civil Engineering, 2018, 2018: 4545891.
[35] LI Xi-bing, CHEN Zheng-hong, WENG Lei, LI Chong-jin. Unloading responses of pre-flawed rock specimens under different unloading rates [J]. Transactions of Nonferrous Metals Society of China, 2019, 29(7): 1516−1526.
[36] HUANG Qing-xiang, ZHENG Chao. Theory of self-stable ring in roadway support [J]. Rock and Soil Mechanics, 2016, 37(5): 1231−1236. (in Chinese)
[37] ZHANG Qi, ZHU He-hua, ZHANG Lian-yang. Modification of a generalized three-dimensional Hoek–Brown strength criterion [J]. International Journal of Rock Mechanics and Mining Sciences, 2013, 59: 80−96.
[38] LI Xi-bing, LI Chong-jin, CAO Wen-zhuo, TAO Ming. Dynamic stress concentration and energy evolution of deep-buried tunnels under blasting loads [J]. International Journal of Rock Mechanics and Mining Sciences, 2018, 104: 131−146.

二步骤回采采场顶板拱架模型及充填接顶率优化

陶 明，赵 岩，过 江

中南大学 资源与安全工程学院，长沙 410083

摘 要：为了探究深部矿山采空区内充填体的合理接顶率，以二步骤回采矿山为例，应用三铰拱力学模型推导回采过程中具有不同接顶率的采空区顶板的应力表达式，并结合数值模拟分析接顶率对采场顶板应力状态的影响。结果表明，竖向应力影响矿房和矿柱采场顶板的应力状态，而水平应力主要影响矿房采场顶板的应力状态。矿房采场充填接顶率对矿柱采场顶板自稳平衡拱的形成有较大的影响。在冬瓜山铜矿开采过程中，现场实际充填接顶率约为 80%，实现了矿产资源安全、稳定的连续回采。

关键词：拱形力学模型；充填接顶率；顶板稳定性；数值模拟；二步骤回采

(Edited by Wei-ping CHEN)